

For the cw PL measurements, the samples were mounted on a piezo-controlled micro-positioning stage allowing each array to be probed individually. The QWs were pumped at normal incidence using light from a 375-nm laser diode, which was passed through a wavelength-selective beamsplitter and then focused onto the sample from the substrate side using a long-working-distance $20\times$ objective lens. The focused spot size was measured with the knife-edge method and found to be approximately $25\ \mu\text{m}$. The PL signal was collected using the same objective lens and beamsplitter, and then analyzed using a fiber-coupled Ocean Optics grating spectrometer. In each set of measurements, an array was initially aligned to the focusing lens using a microscope, and PL spectra were then measured from the regions below the array and adjacent to it by carefully translating the sample.

Time-resolved PL (TRPL) studies were also carried out, in order to evaluate the decrease in recombination lifetime brought about by the silver NPs and in the process confirm the plasmonic origin of the observed PL intensity enhancement. In these measurements the samples were pumped with ultrafast pulses having 100-fs duration and 430-nm center wavelength from a frequency-doubled Ti:Sapphire laser (Spectra Physics Mai-Tai). The emitted light was then detected and analyzed with a Hamamatsu streak camera. Relatively large ($\sim 1\times 1\ \text{mm}^2$) compilations of closely-spaced identical NP arrays were fabricated for these studies, due to the limited spatial resolution of the TRPL setup.

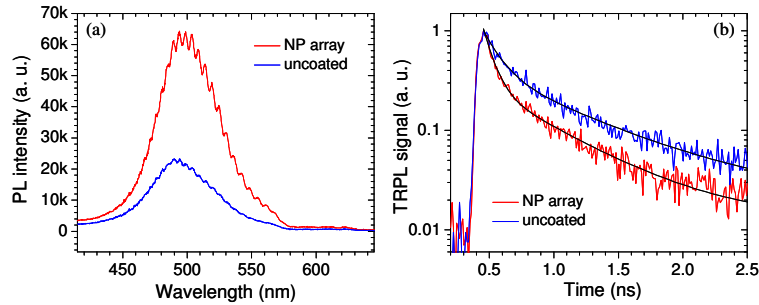


Fig. 2. PL spectra (a) and TRPL signals (b) measured from an uncoated region of the QW sample under study (blue lines) and from the region underneath an array of Ag NPs with 120-nm diameter, 160-nm pitch, and 55-nm height (red lines).

Finally, we also measured the optical transmission spectra of the NP arrays used to demonstrate PL enhancement, which provide direct information about their plasmonic response. To that purpose, the same arrays were fabricated on bulk GaN films grown on sapphire, i.e., without the QWs that would otherwise provide strong optical absorption in the spectral range of interest. The transmission spectra were measured by broadband illumination at normal incidence using unpolarized light from a deuterium tungsten halogen source, with the sample again mounted on a piezo-controlled stage between two $20\times$ objectives. To isolate the extinction features due to the NP arrays only, all measured spectra were normalized to the transmittance of the bare GaN template on sapphire.

3. Results and discussion

The demonstration of plasmon-enhanced near-green light emission using EBL-fabricated NPs is illustrated in Fig. 2. In Fig. 2(a) we show two PL spectra measured from an uncoated region of the QW sample (blue line) and from the region underneath an array of Ag nanocylinders with 120-nm diameter, 160-nm pitch, and 55-nm height (red line). Proximity to the NPs clearly results in a substantial increase in PL intensity, by a factor $r_{\text{PL-I}}$ of nearly 2.8 in this case based on the emission-spectra peak values. In Fig. 2(b) the blue and red lines are the measured TRPL signals (near the wavelength of peak emission) from the bare QWs and from underneath an identical array, respectively. As shown by the black lines in this figure, both traces are in excellent agreement with numerical fits based on a double exponential decay model, where the slower lifetime is related to the recovery of the quantum-confined Stark effect from carrier screening [17], while the faster time constant accounts for radiative and

nonradiative exciton recombination. A pronounced decrease in the latter lifetime is observed in going from the bare QWs to the array-coated region, from 123 to 74 ps based on the fitting curves.

These observations are in full agreement with a picture of plasmon-enhanced light emission. Due to the spatial proximity and relatively close spectral match between the QW excitons and the NP plasmonic excitations, efficient recombination via SPP emission occurs in the sample region below the array, and the TRPL decay lifetime is correspondingly shortened. As a result, fewer carriers are “wasted” through nonradiative recombination processes and the IQE is correspondingly increased. A sufficiently large fraction of the emitted SPPs are then scattered by the NPs into radiation, leading to an overall increase in the measured luminescence.

In order to quantify the various contributions to the observed PL intensity enhancement, we first consider the increase in pump-light reflection coefficient R at the semiconductor-air interface brought about by the NPs. This is an important parameter, since in the backside pumping geometry used in our measurements the pump light intensity absorbed by the QWs is roughly proportional to $1 + R$. To normalize out this effect, the measured PL intensity enhancement should therefore be divided by the factor $f_{refl} = (1 + R_{coat})/(1 + R_{bare})$, where R_{bare} and R_{coat} are the pump reflection coefficients of the bare sample surface and of the array-coated region, respectively. Using Fresnel theory with a refractive index of 2.7 for GaN at the pump wavelength of 375 nm [18], R_{bare} is found to be about equal to 0.21. To estimate R_{coat} , we notice that in the NP array under study the optical transmission at 375 nm is about 56% of its value on the bare surface, as obtained from the measured array transmission spectrum (shown in Fig. 4 below). Assuming that this decrease in transmission is entirely due to increased reflection (both specular and diffuse), we can write $(1 - R_{coat})/(1 - R_{bare}) = 56\%$ and then solve for R_{coat} ; this gives $R_{coat} = 0.56$ and thus $f_{refl} = 1.3$. In practice, the observed decrease in transmission is partly due to optical absorption in the NPs, so that this estimate of f_{refl} should be regarded as an upper limit. Based on this analysis we can therefore conclude that the peak PL intensity in Fig. 2(a) has been enhanced through plasmonic interactions by a factor r_{PL-A}/f_{refl} of at least 2.1.

The underlying increase in IQE can be evaluated from the TRPL measurement results. The IQE of the uncoated QWs depends on the radiative and nonradiative recombination rates (Γ_{rad} and Γ_{nr} , respectively) as $\eta_{int} = \Gamma_{rad}/(\Gamma_{rad} + \Gamma_{nr})$. In the near field of the NP arrays, the IQE becomes

$$\eta'_{int} = \frac{\Gamma_{rad} + \Gamma_{SPP}}{\Gamma_{rad} + \Gamma_{SPP} + \Gamma_{nr}} = \frac{F\Gamma_{rad}}{F\Gamma_{rad} + \Gamma_{nr}}, \quad (1)$$

where Γ_{SPP} is the recombination rate due to emission of SPPs, and the effective Purcell factor $F \equiv (\Gamma_{rad} + \Gamma_{SPP})/\Gamma_{rad}$ is a measure of the average electromagnetic field-intensity enhancement produced by the NPs in the QWs [14]. Not included in Eq. (1) is nonradiative decay via direct near-field excitation of electronic transitions in the metal, which can generally be neglected in the case of semiconductor radiative media [9]. The parameter η_{int} can be estimated from the ratio of the measured PL signals at room temperature and near 10 K [19]; using this procedure, we obtained a value of about 8% for the QW sample under study. The exciton recombination lifetimes obtained from the blue and red TRPL traces of Fig. 2(b) correspond to the reciprocals of $\Gamma_{rad} + \Gamma_{nr}$ and $F\Gamma_{rad} + \Gamma_{nr}$, respectively. Using these experimental quantities in the definitions of η_{int} and η'_{int} and then solving for the remaining parameters, we obtain $F = 8.9$ and $\eta'_{int}/\eta_{int} = 5.4$. This large increase in IQE is partially offset by the finite absorption losses (and hence non-unity scattering efficiency) of the emitted SPPs in the NPs, leading to the smaller measured enhancement in overall PL efficiency.

Next we investigate how the measured plasmon-enhanced luminescence depends on the array geometry. In the case of square arrays of Ag nanocylinders, the key design parameters are the NP diameter D and height H , and the minimum separation S between nearest neighbors. In the following, various combinations of values of D and H are investigated. On

the other hand, S is kept fixed at a reasonably small value of 40 nm, motivated by the importance of producing a strong exciton/SPP coupling over a large fraction of the sample area while at the same time leaving sufficient space between neighboring NPs to eventually allow for convenient device integration via epitaxial overgrowth. On a more fundamental level, the use of ultras small separations S on the order of a few nanometers is also interesting as it is expected to result in particularly large local field enhancements [20], and will be the subject of future studies.

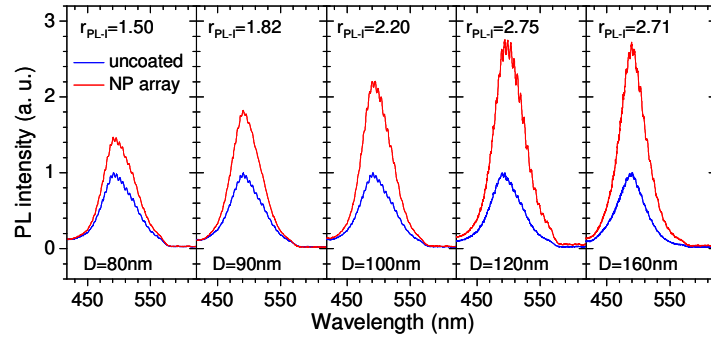


Fig. 3. PL spectra measured with arrays of different NP diameter D (red lines) and from nearby uncoated regions of the same sample (blue lines). In each panel, both spectra are normalized to the peak value of the blue trace.

The observed dependence on diameter is summarized in Figs. 3 and 4 for the case of NPs with a height of approximately 55 nm. In Fig. 3 we plot a representative set of PL spectra measured with arrays of different NP diameter ranging from 80 to 160 nm (red lines). The blue lines are simultaneously measured emission spectra from nearby uncoated regions of the same sample. In each case the NP array produces a significant increase in peak intensity, by a factor r_{PL-I} whose value is also listed in the figure. Specifically, these quoted values are averages over several measurements with nominally identical arrays fabricated in the same run; the associated standard deviations are typically below 10%. As shown in this figure, r_{PL-I} initially increases with diameter from 1.5 for $D = 80$ nm until it reaches a maximum value of nearly 2.8 near $D = 120$ nm. As D is further increased, r_{PL-I} is found to saturate; at the same time, the sample-area coverage with Ag increases, which eventually may complicate the further integration of the NPs in a full device structure via epitaxial overgrowth.

In Fig. 4 we show the normalized transmission spectra of the same array geometries. A pronounced dip is seen in each case, associated with the main plasmonic resonance of the respective array. For $D = 80$ nm, this feature is centered relatively close to the QW emission wavelength. As D is increased it red-shifts and broadens as expected [16], while a second dip due to a higher-order SPP mode develops at shorter wavelengths and similarly broadens.

The observed PL-intensity variations in Fig. 3 are mainly the result of two conflicting mechanisms. On the one hand, as D is increased the array main plasmonic resonance red-shifts away from the QW emission wavelength, and therefore the exciton/SPP resonant coupling decreases. On the other hand, in general larger NPs feature larger plasmonic scattering efficiency [16], which is evidenced in Fig. 4 by the increasing strength and width of the measured transmission dips with increasing diameter. As D is increased, more and more of the emitted SPPs are therefore scattered into radiation and contribute to the measured PL signal, as opposed to being absorbed in the metal. The enhancement data of Fig. 3 indicate that this latter mechanism is dominant up to around $D = 120$ nm, causing an overall increase in PL intensity with increasing diameter. Incidentally, the NP area coverage also increases with diameter in the arrays of Fig. 3; however, simple geometrical considerations show that this effect can only account for a small fraction of the observed PL-intensity variations. It should be noted that the key role played by scattering efficiency in this context is a direct consequence of the relatively short wavelengths used, which require comparatively small (and

therefore lossy) nanocylinders. For the same reason, even larger enhancements should be expected using similar arrays with samples emitting at longer wavelengths.

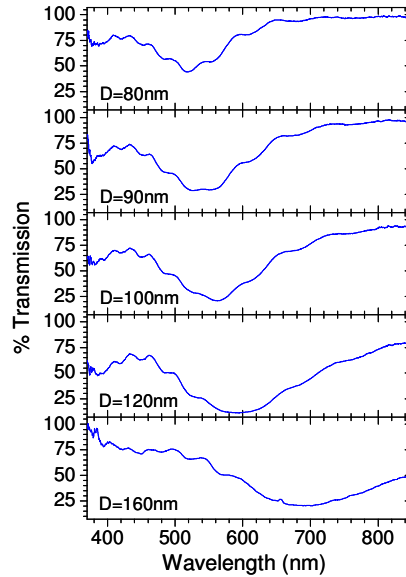


Fig. 4. Normalized transmission spectra of the same array geometries of Fig. 3 fabricated on a GaN film.

Another important feature of the transmission spectra of Fig. 4 is the appearance of a higher-order shorter-wavelength plasmonic excitation. This resonance may also couple to the light-emitting excitons in the QWs and therefore contribute to the PL-intensity enhancement, especially in the larger-diameter arrays. Furthermore, due to its spectral overlap with the pump wavelength of 375 nm, it is likely to cause some dissipation of the incident pump light in the PL measurements in addition to reflection and scattering back into the QWs. As a result, the aforementioned estimate of the pumping-efficiency correction factor f_{refl} based on the transmission data should be regarded as an upper limit. Incidentally, in the case of the arrays of Figs. 3 and 4 this estimate of f_{refl} is found to vary over the small range 1.1–1.3.

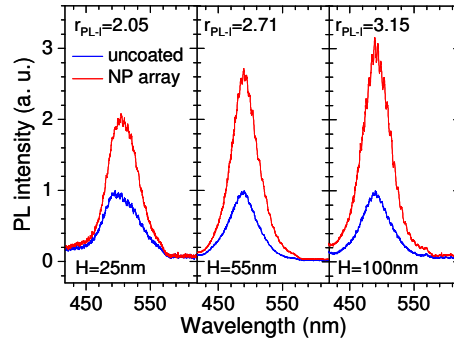


Fig. 5. PL spectra measured with arrays of different NP height H (red lines) and from nearby uncoated regions of the same sample (blue lines). In each panel, both spectra are normalized to the peak value of the blue trace.

Finally, in Figs. 5 and 6 we show the PL and transmission spectra, respectively, measured with three arrays of equal NP diameter D (160 nm) and equal nearest-neighbor spacing S (40 nm) but different NP height H (25, 55, and 100 nm). As shown in Ref [15], the plasmonic

resonance of square arrays of Ag nanocylinders can be effectively blue-shifted by increasing the NP height, while at the same time maintaining small optical absorption losses. As a result, taller NPs in the present context can provide a more favorable tradeoff between the requirements of strong exciton/SPP resonant coupling and efficient SPP scattering. These expectations are confirmed by the data of Figs. 5 and 6. Specifically, as the NP height is increased from 25 to 100 nm, the main plasmonic resonance wavelength shifts from about 765 to 665 nm, while the average PL-intensity enhancement factor $r_{\text{PL-I}}$ (listed in Fig. 5) increases from 2.1 to over 3.1. The latter value is the largest enhancement observed in all the arrays considered in this work; using the correction factor $f_{\text{refl}} = 1.3$ estimated from the $H = 100$ -nm transmission spectrum of Fig. 6, we obtain a lower bound for the plasmonic contribution to this enhancement of over 2.5. Additional improvements may be possible using even taller NPs; however this has been limited by a decreasing yield in our liftoff process on the GaN surface with increasing metal thickness (particularly due to the small particle spacings involved), and will require further process development.

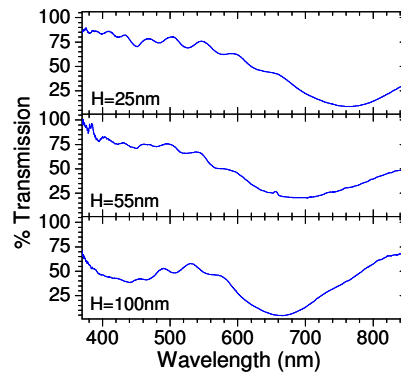


Fig. 6. Normalized transmission spectra of the same array geometries of Fig. 5 fabricated on a GaN film.

4. Summary

In conclusion, we have demonstrated plasmon-enhanced near-green light emission from InGaN/GaN QWs using Ag NP arrays fabricated by EBL. Several arrays with different NP dimensions were developed and used to produce large enhancements in peak PL intensity. The underlying physical mechanism is the resonant coupling between the QW excitons and the NP plasmonic excitations (which was directly demonstrated and quantified via TRPL measurements), followed by efficient scattering of the emitted SPPs into radiation. The experimental PL-intensity enhancement factors were found to vary over a wide range depending on the array geometry, e.g., from about 1.5 in the smallest-diameter array of Fig. 3 to over 3.1 in the largest-height array of Fig. 5. This observation highlights the importance of properly designing the array geometry for optimal light-emission efficiency enhancement. The arrays studied in this work can be integrated within a full LED device, e.g., by epitaxial overgrowth, and therefore are promising for the development of solid-state light sources of highly improved efficiency.

Acknowledgements

This work was supported by the Department of Energy under Grant No. DE-FG02-06ER46332. Partial support by the AFOSR Awards FA9550-10-1-0019 and FA9550-06-1-0470 is also acknowledged.